nature chemical biology

ARTICLE

PUBLISHED ONLINE: 6 MARCH 2017 | DOI: 10.1038/NCHEMBIO.2307

L-2-Hydroxyglutarate production arises from noncanonical enzyme function at acidic pH

Andrew M Intlekofer[1,2], Bo Wang[1], Hui Liu[3], Hardik Shah[3], Carlos Carmona-Fontaine[4], Ariën S Rustenburg[4], Salah Salah[5], M R Gunner[5], John D Chodera[4], Justin R Cross[3] & Craig B Thompson[1]*

The metabolite 2-hydroxyglutarate (2HG) can be produced as either a D-*R*- or L-*S*- enantiomer, each of which inhibits α-ketoglutarate (αKG)-dependent enzymes involved in diverse biologic processes. Oncogenic mutations in isocitrate dehydrogenase (IDH) produce D-2HG, which causes a pathologic blockade in cell differentiation. On the other hand, oxygen limitation leads to accumulation of L-2HG, which can facilitate physiologic adaptation to hypoxic stress in both normal and malignant cells. Here we demonstrate that purified lactate dehydrogenase (LDH) and malate dehydrogenase (MDH) catalyze stereospecific production of L-2HG via 'promiscuous' reduction of the alternative substrate αKG. Acidic pH enhances production of L-2HG by promoting a protonated form of αKG that binds to a key residue in the substrate-binding pocket of LDHA. Acid-enhanced production of L-2HG leads to stabilization of hypoxia-inducible factor 1 alpha (HIF-1α) in normoxia. These findings offer insights into mechanisms whereby microenvironmental factors influence production of metabolites that alter cell fate and function.

The discovery of oncogenic mutations in IDH enzymes demonstrated the profound impact that altered metabolism can have on cell identity and function[1,2]. Mutant IDH enzymes efficiently catalyze reduction of αKG to the 'oncometabolite' D-2HG[3,4]. D-2HG inhibits a large family of >70 different αKG-dependent enzymes that regulate chromatin modifications, stability of HIFs, extracellular-matrix maturation, and DNA repair[1]. In particular, D-2HG-mediated inhibition of chromatin-modifying enzymes impairs induction of gene expression programs that are required for normal cell differentiation and 'locks' malignant cells in an undifferentiated stem-cell-like state[5–7]. The relative contributions of different D-2HG targets to oncogenesis likely vary depending on the cellular context[8,9].

While intensive efforts have been directed at investigating the molecular and cellular effects of IDH-mutant-derived D-2HG, potential sources and functions of the mirror-image enantiomer L-2HG are less well understood[10]. Importantly, biochemical assays demonstrated that L-2HG functions as a more potent inhibitor of αKG-dependent enzymes than D-2HG; thus, cells may be quantitatively more sensitive to changes in L-2HG than to changes in D-2HG[11–13]. Indeed, deregulated L-2HG disposal causes substantial developmental pathology and is associated with brain and kidney cancers[14–16].

It was recently reported that hypoxia induces production of L-2HG in both normal and malignant cells as a physiologic response to oxygen limitation[17,18]. Hypoxia-induced production of L-2HG occurs independently of HIF but acts to reinforce the hypoxic response, at least in part, through stabilization of HIF protein[13,17,18]. Accumulation of L-2HG slows glycolysis and mitochondrial respiration by reducing the rate of regeneration of NAD^+ (ref. 18). Moreover, hypoxia-induced L-2HG promotes the same repressive chromatin marks that characterize the differentiation blockade of IDH-mutant malignancies[8,17,19], consistent with the well-established association between hypoxic niches and stem-cell populations[20].

Genetic evidence suggests that LDH and MDH enzymes are major sources of hypoxia-induced L-2HG[16–18,21], but there has been no confirmation that these enzymes directly catalyze L-2HG production. Here we demonstrate that purified LDH and MDH enzymes can catalyze stereospecific reduction of αKG to L-2HG and that acidic reaction conditions dramatically enhance LDH- and MDH-mediated production of L-2HG *in vitro* and in cells. Mechanistically, acidic pH enhances lactate dehydrogenase A (LDHA)-mediated reduction of αKG by driving equilibrium toward a protonated form of αKG that binds more stably to the LDHA enzyme. In living cells, the pH-dependent induction of L-2HG acts as a potent stabilizer of HIF-1α in normoxia, representing a previously unknown pathway of HIF-1α stabilization that has potential relevance to human disease states. These findings offer new insights into the mechanisms that regulate noncanonical substrate use by metabolic enzymes and the consequences of promiscuous L-2HG production in cell physiology.

RESULTS

LDH and MDH enzymes use αKG as an alternative substrate

Hypoxic cells undergo a number of metabolic changes (**Fig. 1a**) including an increased NADH to NAD^+ ratio[18,22], an increased intracellular concentration of αKG[18,23], and acidification of the extracellular and intracellular environments[24,25]. Prior reports implicated LDHA and malate dehydrogenase 1 and 2 (MDH1 and MDH2) as being contributors to hypoxia-induced L-2HG in cells (**Fig. 1a**)[17,18]. To determine whether these enzymes could directly produce L-2HG, we tested the ability of purified LDH and MDH to catalyze NADH-dependent reduction of their canonical substrates as well as αKG. As expected, LDH rapidly consumed NADH in the presence of its canonical substrate pyruvate (**Fig. 1b**). LDH also consumed NADH in the presence of αKG, confirming its capacity to utilize alternative, larger α-ketoacid substrates (**Fig. 1b**)[26,27]. Likewise, MDH efficiently catalyzed reduction of its canonical substrate oxaloacetate (OAA; **Fig. 1c**), while also demonstrating an ability to use αKG as a noncanonical substrate, albeit less efficiently (**Fig. 1c**).

[1]Cancer Biology and Genetics Program, Memorial Sloan Kettering Cancer Center, New York, New York, USA. [2]Department of Medicine, Memorial Sloan Kettering Cancer Center, New York, New York, USA. [3]The Donald B. and Catherine C. Marron Cancer Metabolism Center, Memorial Sloan Kettering Cancer Center, New York, New York, USA. [4]Computational Biology Program, Memorial Sloan Kettering Cancer Center, New York, New York, USA. [5]Physics Department, City College of New York, New York, New York, USA. *e-mail: thompsonc@mskcc.org

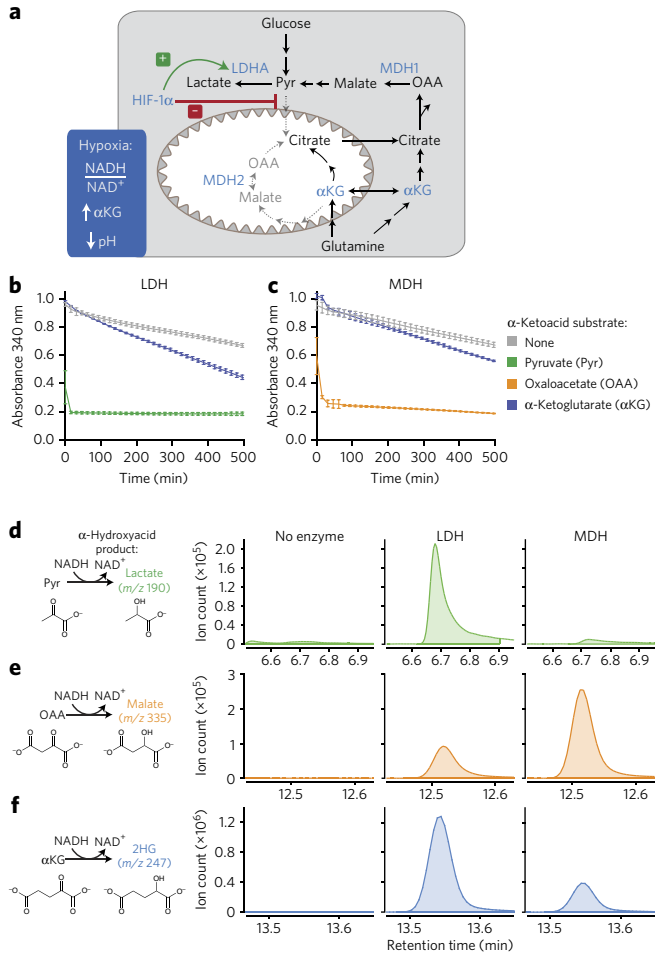

Figure 1 | LDH and MDH enzymes catalyze reduction of the alternative substrate αKG. (**a**) Schematic of metabolic changes that occur in hypoxic cells. Lactate dehydrogenase A (LDHA) and malate dehydrogenase 1 and 2 (MDH1 and MDH2) represent potential enzymatic sources of L-2-hydroxyglutarate (L-2HG) production in cells. αKG, α-ketoglutarate; HIF-1α, hypoxia-inducible factor 1 alpha; OAA, oxaloacetate. (**b**) Enzyme assay measuring NADH consumption by LDH purified from bovine heart (5 units/ml) in reactions with no substrate (gray), 0.3 mM pyruvate (green), or 1 mM αKG (blue). (**c**) NADH consumption by MDH purified from porcine heart (5 units/ml) in reactions with no substrate (gray), 0.3 mM OAA (orange), or 3 mM αKG (blue). Data in **b** and **c** are shown as the mean ± 95% confidence interval (c.i.) for triplicate reactions. (**d**–**f**) α-Hydroxyacid product formation catalyzed by dehydrogenases. GC–MS analysis of lactate production from pyruvate (**d**), malate production from OAA (**e**), and 2HG production from αKG (**f**) in 6-h reactions with no enzyme, LDH purified from bovine heart (10 μg/ml), or MDH purified from porcine heart (10 μg/ml). Reactions were conducted in 33 mM potassium phosphate buffer, pH 7.0, with 0.22 mM NADH. Results throughout the figure are representative of ≥3 independent experiments.

We performed gas chromatography–mass spectrometry (GC–MS) to determine the identities of the α-hydroxyacid reaction products generated by LDH and MDH enzymes. Analysis of reaction mixtures without enzyme demonstrated that there was no significant nonenzymatic production of lactate, malate, or 2HG (**Fig. 1d–f**). LDH, but not MDH, catalyzed reduction of pyruvate to lactate (**Fig. 1d**). Both MDH and LDH catalyzed reduction of OAA to malate, with MDH catalyzing this reaction more efficiently than LDH, as expected (**Fig. 1e**). Notably, both LDH and MDH enzymes were capable of promiscuously catalyzing NADH-dependent reduction of the alternative substrate αKG to 2HG (**Fig. 1f**).

LDH and MDH catalyze reduction of αKG to L-2HG

Standard metabolite derivatization and chromatography methods do not distinguish between enantiomeric species. In order to separate α-hydroxyacid enantiomers, we adapted a liquid chromatography–mass spectrometry (LC–MS) protocol involving derivatization of metabolites with the chiral compound diacetyl-L-tartaric anhydride (**Supplementary Results** and **Supplementary Fig. 1**)[28]. The identity of α-hydroxyacid enantiomers was confirmed by comparison to similarly derivatized standards (**Fig. 2a–c**). As expected, chiral derivatization showed that LDH catalyzed reduction of pyruvate to L-lactate, whereas MDH catalyzed this reaction poorly (**Fig. 2a**). MDH catalyzed its canonical reaction involving reduction of OAA to L-malate (**Fig. 2b**), while LDH catalyzed this reaction less effectively (**Fig. 2b**). Both LDH and MDH catalyzed stereospecific reduction of αKG to L-2HG (**Fig. 2c** and **Supplementary Fig. 2**). To ensure that L-2HG production was not facilitated by an unknown contaminant of the enzyme preparations (**Supplementary Fig. 3a**), we also studied recombinant human LDHA, MDH1, and MDH2 enzymes. The recombinant enzymes also catalyzed stereospecific reduction of αKG to L-2HG (**Supplementary Fig. 3b–f**). Collectively, these findings substantiate genetic evidence suggesting that LDH and MDH enzymes contribute to cellular production of L-2HG[16–18,21].

Wild-type IDH and PHGDH enzymes produce D-2HG

Prior reports demonstrated that wild-type IDH enzymes can catalyze reduction of αKG to 2HG, but the stereochemistry of the 2HG product was not determined[29,30]. Therefore, we sought to assess whether wild-type IDH enzymes might represent another cellular source of D- or L-2HG. Using a cell-based assay, we observed that transfection with empty vector had no effect on D- or L-2HG levels, whereas transfection with wild-type IDH1 or IDH2 selectively increased D-2HG levels (**Supplementary Figs. 4a**,**b** and **5**). Supplementation with cell-permeable αKG substrate resulted in a further increase in the amount of D-2HG in cells transfected with wild-type IDH1 or IDH2 (**Supplementary Figs. 4a**,**b** and **5**), albeit the increase was ~50- to 100-fold less than that observed in cells transfected with an oncogenic IDH1 R132H mutant (**Supplementary Fig. 4c**).

Commercially available preparations of IDH from porcine heart were impure and thus unsuitable for enzymatic assays, prompting us to use recombinant human IDH1 as an alternative (**Supplementary Fig. 3a**). Employing previously reported reaction conditions with Tris-based buffers[31], we detected substantial nonenzymatic production of 2HG that was equally distributed as D- and L- enantiomers (**Supplementary Fig. 6**). By contrast, nonenzymatic 2HG production was negligible in phosphate-based reaction buffers (**Supplementary Fig. 6**). Using phosphate-based buffers, we found that recombinant human IDH1 selectively catalyzed production of D-2HG (**Supplementary Fig. 4d**). Taken together, the cell-based and recombinant enzyme assays demonstrate that wild-type IDH enzymes can catalyze production of D-2HG, an intrinsic enzymatic property that is substantially enhanced by the active site arginine residue mutations in IDH that are observed in cancer[29,30].

The enzyme 3-phosphoglycerate dehydrogenase (PHGDH) was recently identified as another potential cellular source of D-2HG[32,33]. Indeed, we found that recombinant human PHGDH catalyzed stereospecific reduction of αKG to D-2HG *in vitro* (**Supplementary Fig. 4e**). The locus encoding PHGDH is frequently amplified in breast cancer and melanoma[34,35], and elevated 2HG levels have been detected in primary breast tumors with aggressive features but no IDH mutation[36]. Thus, determining the chirality of 2HG should help elucidate which metabolic pathway contributes to 2HG production in various cancer settings.

Acidic pH enhances the alternative enzymatic activity of LDH

While investigating the enzymatic properties of LDH, we noted a striking enhancement in NADH-dependent reduction of αKG

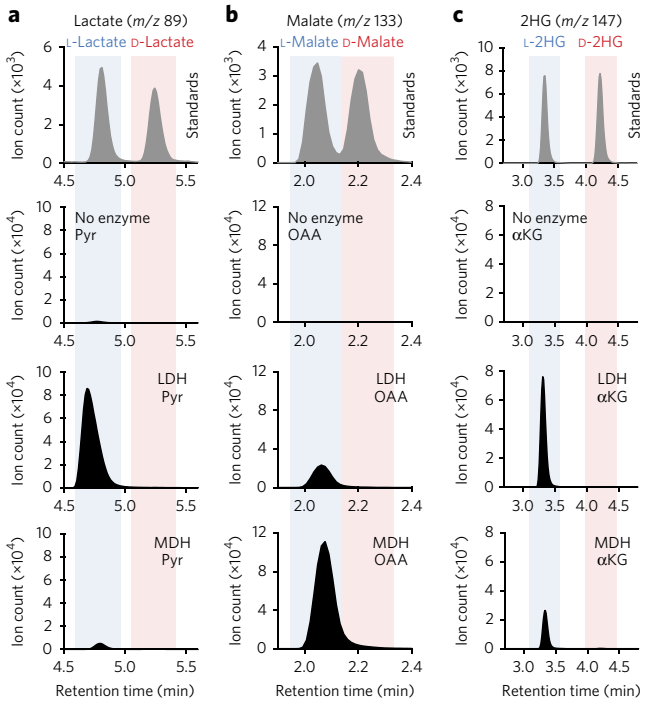

Figure 2 | LDH and MDH selectively produce L-α-hydroxyacids, including L-2HG. (**a**–**c**) Chiral LC–MS analysis resolving enantiomers of lactate produced from pyruvate (**a**), malate produced from OAA (**b**), and 2HG produced from αKG (**c**) in 6-h reactions with no enzyme, LDH purified from bovine heart (5 units/ml), or MDH purified from porcine heart (5 units/ml) in 33 mM potassium phosphate buffer, pH 7.0, with 0.22 mM NADH and 1 mM substrate. The top panels show mixtures of standards for L- and D- enantiomers of lactate, malate, and 2HG that were derivatized and analyzed by the same method in parallel. Vertical blue and red bars in the background serve as visual references to facilitate the identification of L- and D- enantiomers, respectively. Results throughout the figure are representative of ≥3 independent experiments.

at more acidic pH (**Fig. 3a**). Specifically, the K_m of LDH for αKG decreased from >15 mM at pH 7.4 to 3.86 ± 0.97 mM at pH 6.0 (**Fig. 3b**), a value that approximates the concentration of αKG in hypoxic cells[18]. We found that the enhanced rate of αKG-dependent NADH consumption at more acidic pH resulted in increased LDH-dependent production of L-2HG (**Fig. 3c**). Acidification also enhanced the ability of MDH to catalyze reduction of αKG to L-2HG, albeit to a lesser degree (**Fig. 3d–f**). Although the rate of nonenzymatic NADH degradation increased at acidic pH, there was no detectable nonenzymatic production of L-2HG (**Supplementary Fig. 7**).

In contrast to the effects on noncanonical substrate usage, acidic pH had no substantial effect on the ability of LDH to reduce its canonical substrate pyruvate at a near physiologic pyruvate concentration of 0.3 mM (**Fig. 3g**)[37]. At concentrations of pyruvate greater than 0.3 mM, acidic pH impaired the ability of LDH to reduce pyruvate because of enhanced substrate inhibition, as previously described (**Fig. 3g,h**)[38]. Together, these results demonstrate that acidification enhances the alternative substrate utilization of LDH such that the noncanonical substrate αKG is relatively favored at lower pH, resulting in increased production of L-2HG.

We also examined the effects of acidic pH on the ability of wild-type IDH1 and PHGDH to reduce αKG to D-2HG. Wild-type IDH1 exhibited minimal pH-dependent change in D-2HG production (**Supplementary Fig. 8a**). In contrast, PHGDH exhibited enhanced D-2HG production in acidic pH (**Supplementary Fig. 8b**).

Acidity enhances reduction of a subset of α-ketoacids

To determine whether acidic pH might increase accessibility to the substrate-binding pocket of LDH, we tested the effect of pH on LDH-mediated reduction of α-ketoacids with bulky tail groups, including phenylpyruvate (PP) and hydroxyphenylpyruvate (HPP) (**Fig. 4a**). We observed that LDH reduced both PP and HPP at a rate at least as great as that of αKG, and there were no substantial pH-dependent changes in the rate of reduction for either substrate (**Fig. 4a**). These findings suggest that acidic pH does not function merely to enhance access for substrates larger than pyruvate, such as αKG, to the substrate-binding pocket of LDH.

We investigated whether the nature of the chemical moiety present in the tail end of the α-ketoacid substrate might dictate the pH-dependent properties of the LDH enzymatic reaction. We identified pairs of α-ketoacid substrates of identical carbon chain length that differed only in whether there was a carboxylate or methyl group present in the final position (**Fig. 4b**): OAA (4-carbon), αKG (5-carbon), and oxoadipic acid (OAdA; 6-carbon) along with their respective methylated counterparts α-ketobutyrate (αKB; 4-carbon), oxopentanoic acid (OPA; 5-carbon), and ketohexanoic acid (KHA; 6-carbon). For each substrate pair, only the α-ketoacid with a carboxylate group in the final position exhibited pH-dependent enhancement of enzymatic reduction (**Fig. 4b**).

Acidification enhances interaction of αKG with LDHA Q100

We performed Monte Carlo protonation state modeling simulations with virtually docked substrates to determine whether pH-dependent changes in the protonation states of αKG, NADH, or LDHA might be responsible for the acid-enhanced enzymatic reduction of αKG. The docked structure of αKG demonstrated that the carboxylate group in the tail of the substrate is positioned immediately adjacent to glutamine 100 (Q100) in the substrate-binding pocket of LDHA (**Fig. 5a**). Prior reports demonstrated that the corresponding residue in bacterial LDH plays an important role in determining substrate specificity[39,40].

Analysis of the Monte Carlo simulations demonstrated a change of the predominant protonation state of αKG upon binding LDHA with NADH. The carboxylate tail of αKG has a predicted pK_a of 4.28 ± 1.27 (closely matching the experimental pK_a of 4.4)[41], indicating that it would be mostly deprotonated in solution at pH values ranging from 6.0 to 7.4. However, upon binding to LDHA, the carboxylate tail of αKG becomes protonated, whereupon it is predicted to form a hydrogen bond with Q100 (**Fig. 5b**). This is associated with a free-energy penalty for protonating the carboxylate tail that opposes binding, which for a given pH can be expressed as

$$\Delta G_{pH} = k_B T(\mathrm{pH} - pK_a)(\ln 10)$$

where k_B is the Boltzmann constant and T equals the absolute temperature. Protonating the carboxylate tail at pH 7.4 would cost 3.2 $k_B T$ more than protonating it at pH 6.0 (**Fig. 5c**). The expected fold change in the aqueous concentration of the deprotonated form is calculated as follows.

$$\frac{e^{-\Delta G_{6.0}/k_B T}}{e^{-\Delta G_{7.4}/k_B T}}$$

If the enzyme greatly prefers to bind the protonated form, then the predicted K_m of αKG would be approximately 25 times higher (corresponding to lower affinity) at pH 7.4 than at 6.0, lacking additional pH-dependent effects. These predictions are consistent with the increased K_m measured experimentally for αKG at pH 7.4 as compared to pH 6.0 (**Fig. 3c**).

Mutation of Q100 to a positively charged amino acid might alter the substrate preference for LDHA such that it would favor αKG with the carboxylate tail in the deprotonated (negatively charged)

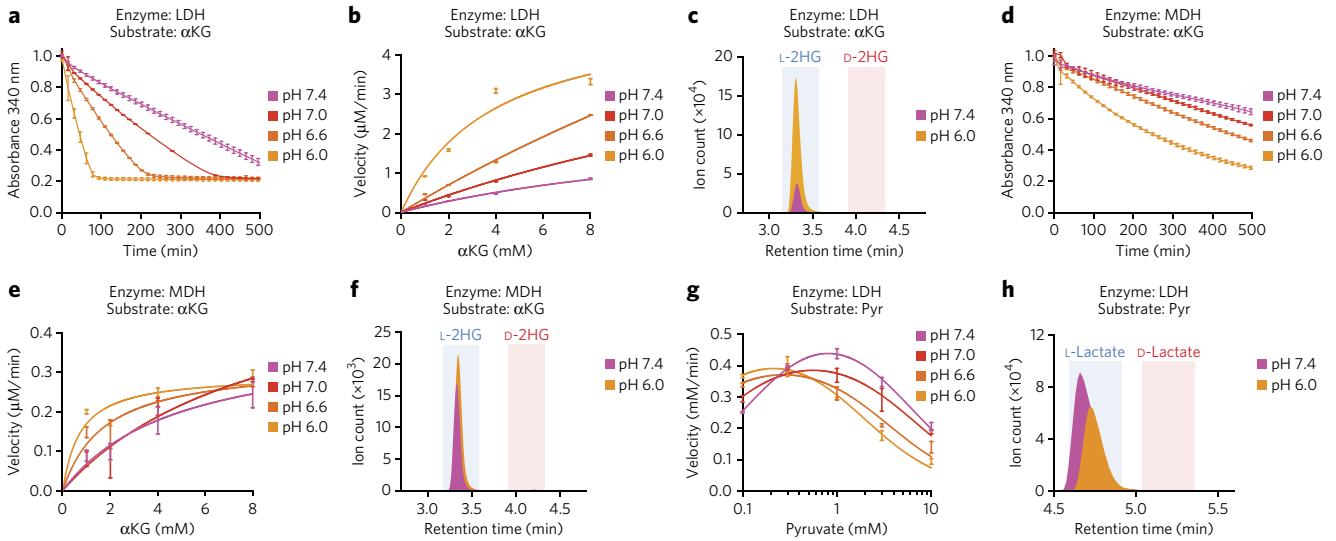

Figure 3 | Acidic pH enhances L-2HG production by LDH and MDH. (**a**–**c**) LDH- and (**d**–**f**) MDH-catalyzed conversion of αKG to L-2HG as a function of pH. (**a**,**d**) Increased rates of NADH consumption in acidic reaction conditions with purified LDH (**a**) or MDH (**d**) at 5 units/ml and 3 mM αKG. Data in **a** and **d** are shown as the mean ± 95% c.i. for triplicate reactions. (**b**,**e**) Reaction velocities as a function of αKG concentration for purified LDH (**b**) or MDH (**e**) at 5 units/ml. (**c**,**f**) Chiral LC–MS analysis of 2HG enantiomers from 6-h reactions with purified LDH (**c**) or MDH (**f**) at 5 units/ml and 1 mM αKG. (**g**) Reaction velocities as a function of pyruvate concentration for purified LDH at 1 μg/ml. (**h**) Chiral LC–MS analysis of lactate enantiomers from 6-h reactions with purified LDH at 5 units/ml and 1 mM pyruvate. Reactions were done in 33 mM potassium phosphate buffer at the indicated pH with 0.22 mM NADH. Data for **b**, **e**, and **g** are shown as the mean ± s.d. for triplicate reactions. Results throughout the figure are representative of ≥3 independent experiments.

state, thus abolishing the pH trend observed with the wild-type LDHA enzyme. Indeed, mutation of the corresponding residue in bacterial LDH from glutamine to arginine (Q102R) enhanced the ability of the enzyme to reduce OAA[39,40]. Therefore, we generated vectors expressing either wild-type LDHA (LDHA WT) or LDHA with a point mutation resulting in replacement of glutamine 100 with arginine (LDHA Q100R). The constructs were transfected into 293T cells, and the FLAG-tagged enzymes were purified by immunoprecipitation (**Supplementary Fig. 9**). Equal quantities of enzyme were used for *in vitro* reactions with NADH cofactor and the substrates αKG, OPA, pyruvate (Pyr), and OAA (**Fig. 5d**–**g**).

In contrast to the acid-enhanced reduction of αKG mediated by wild-type LDHA, the LDHA Q100R mutant exhibited a relatively faster rate of αKG reduction at higher pH values, with no enhancement of activity as the pH decreased (**Fig. 5d**). Thus, the positive charge of the Q100R mutant appears to eliminate the energetic penalty normally required to protonate the carboxylate tail of αKG. By contrast, the LDHA Q100R mutant exhibited relatively impaired enzymatic reduction of OPA, which has a methyl group in the tail position (**Fig. 5f**). Likewise, the LDHA Q100R mutant exhibited a relative preference for OAA (**Fig. 5e**) and a relatively impaired ability to reduce pyruvate (**Fig. 5g**). Taken together, these findings suggest that acidic pH enhances the ability of wild-type LDHA to reduce substrates with a carboxylate group in the final position by diminishing the energetic penalty of protonating the substrate tail to accommodate binding with Q100 in the LDHA substrate-binding pocket. The LDHA Q100R mutant introduces a positively charged residue at the Q100 site, which alters substrate preference such that α-ketoacids with carboxylate tails need not pay the energetic cost of being protonated to bind and are relatively favored at higher pH values.

Acid-enhanced production of L-2HG stabilizes HIF-1α

Given the striking enhancement of LDH-catalyzed L-2HG production observed *in vitro*, we sought to determine the effects of acidification on 2HG production in cells. Glioblastoma cells grown in normoxic conditions were lysed in nondenaturing buffer with pH ranging from 7.5 to 6.0 (**Fig. 6a**). Cell lysates were used as a source of enzyme for *in vitro* reactions with addition of αKG and NADH, and 2HG production was assessed by GC–MS. As the reaction pH was lowered, there was a progressive increase in the amount of 2HG produced such that there was >3-fold more 2HG at pH 6.0 than there was at pH 7.5 (**Fig. 6a**). Assessment of chirality by LC–MS confirmed that acidification of cell-lysate reactions potently induced production of L-2HG (**Fig. 6b**). Acid-enhanced L-2HG production was blocked by addition of oxamate, an LDH inhibitor that is a structural analog of pyruvate (**Fig. 6b**)[42]. Thus, acid-enhanced production of L-2HG depends, at least in part, on the enzymatic activity of LDH.

Hypoxia results in acidification of the cellular environment and an increase in the intracellular concentration of αKG (**Fig. 1a**)[18,23–25], but it is unclear to what extent these conditions might be sufficient to induce production of L-2HG. Therefore, we tested the effects of acidified medium and/or exogenous αKG on cells cultured in normoxia (**Fig. 6c**). As previously reported, addition of cell-permeable αKG resulted in a modest increase in 2HG production in cells cultured in standard medium in normoxia (**Fig. 6c**)[17]. However, we observed a synergistic enhancement of 2HG production in cells cultured in acidified medium supplemented with cell-permeable αKG (**Fig. 6c**). Quantification of the intracellular concentrations of L- and D-2HG demonstrated that L-2HG levels exceeded 0.3 mM in acidified media supplemented with cell-permeable αKG (**Fig. 6d**), approximating previous measurements in hypoxic cells[17,18]. In contrast, D-2HG concentrations were approximately tenfold lower (**Fig. 6d**). Measurement of intracellular pH with fluorescent probes demonstrated a value of pH 6.53 ± 0.29 for cells cultured in acidic medium plus αKG (**Supplementary Fig. 10**).

Cells cultured in acidic medium plus αKG demonstrated a striking stabilization of HIF-1α despite the presence of atmospheric oxygen levels (**Fig. 6c** and **Supplementary Fig. 11**). The observed stabilization of HIF-1α by αKG is paradoxical given the fact that αKG functions as a substrate for the egg-laying deficiency protein nine-like (EGLN) enzymes that hydroxylate proline residues on HIF and target it for proteasomal degradation[43]. Therefore, we examined the effects of acidification plus αKG on the ratio of hydroxyl-HIF-1α to total HIF-1α in 293T cells cultured in the presence of the

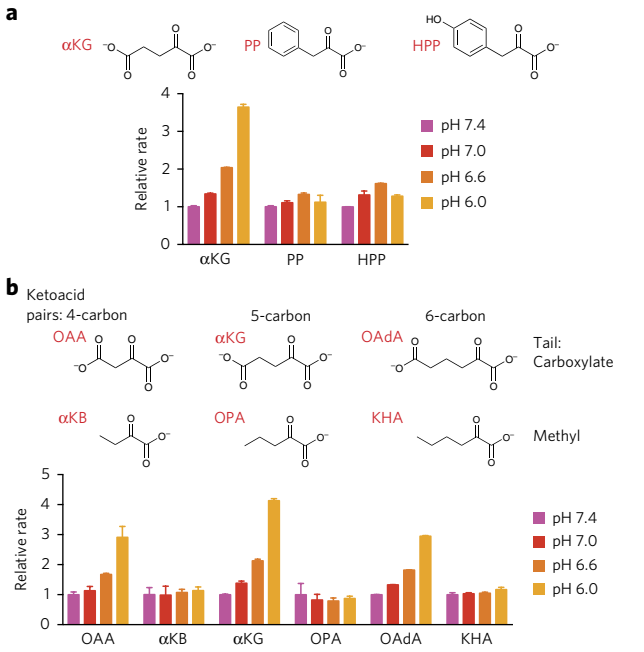

Figure 4 | LDH exhibits pH-sensitive reduction of α-ketoacids with carboxylate tails. (**a**) Relative rates of NADH consumption at the indicated pH with purified LDH at 5 units/ml, 0.22 mM NADH, and 1 mM substrate. For each substrate, the rate at pH 7.4 was normalized to 1 to illustrate the degree of rate enhancement with acidification. Structures for substrates αKG, phenylpyruvate (PP), and hydroxyphenylpyruvate (HPP) are shown. (**b**) Relative rates of NADH consumption at the indicated pH with purified LDH at 5 units/ml, 0.22 mM NADH, and 1 mM substrate. For each substrate, the rate at pH 7.4 was normalized to 1 to illustrate the degree of rate enhancement with acidification. Structures are shown for α-ketoacid substrates with carboxylate tails, OAA, αKG, and oxoadipic acid (OAdA), along with their respective methylated counterparts, α-ketobutyrate (αKB), oxopentanoic acid (OPA), and ketohexanoic acid (KHA). Data are shown as the mean ± s.d. for triplicate reactions. Results throughout the figure are representative of ≥3 independent experiments.

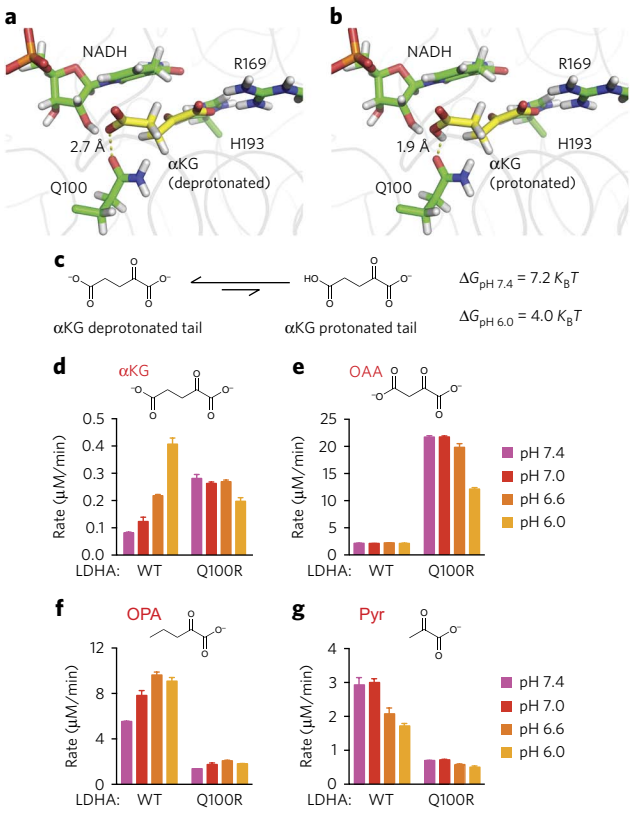

Figure 5 | Acidity-induced rate enhancement arises from preference of LDHA for the protonated form of αKG. (**a**) Virtually docked structure of deprotonated αKG (yellow) bound to LDHA, showing a potentially unfavorable interaction between the carbonyl of the Q100 residue and the tail of αKG. (**b**) Virtually docked structure of protonated αKG (yellow) bound to LDHA, showing a potential hydrogen bond interaction between the carbonyl of the Q100 residue and the protonated carboxylate tail of αKG, predicted to be the dominant bound species by Monte Carlo simulations. (**c**) The equilibrium of protonation states of the tail of αKG in solution. Shown on the right is the theoretical free-energy penalty of protonating the tail at pH 7.4 ($\Delta G_{pH\ 7.4}$) and pH 6.0 ($\Delta G_{pH\ 6.0}$) in units of k_BT, in which k_B is the Boltzmann constant and T is the absolute temperature. (**d**–**g**) Wild-type (WT) or mutant (Q100R) LDHA enzymes were purified and used in enzymatic reactions with α-ketoglutarate (αKG) (**d**), oxaloacetate (OAA) (**e**), oxopentanoic acid (OPA) (**f**), or pyruvate (Pyr) (**g**). Reactions were performed in 33 mM potassium phosphate buffer at the indicated pH with 0.22 mM NADH and 1 mM substrate and with enzyme at 7 μg/ml (**d**,**f**), 0.7 μg/ml (**e**), or 0.07 μg/ml (**g**). Data for **d**–**g** are shown as the mean ± s.d. for triplicate reactions. Results throughout the figure are representative of ≥3 independent experiments.

proteasome inhibitor MG132 (**Fig. 6e** and **Supplementary Fig. 11**)[44]. Cells cultured in standard medium plus MG132 accumulated hydroxyl-HIF-1α relative to total HIF-1α in response to cell-permeable αKG (**Fig. 6e** and **Supplementary Fig. 11**). In contrast, cells cultured in acidified medium plus MG132 did not accumulate hydroxyl-HIF-1α despite a substantial increase in total HIF-1α protein (**Fig. 6e** and **Supplementary Fig. 11**). Thus, we conclude that acid-enhanced L-2HG production stabilizes HIF-1α by inhibiting the αKG-dependent prolyl hydroxylases that target HIF-1α for degradation, in agreement with previously observed effects of L-2HG on prolyl hydroxylases *in vitro*[11,13].

To further explore the possibility that acid-enhanced L-2HG lies upstream of HIF-1α, we tested the effects of ablating LDHA and MDH2, the two enzymes primarily responsible for L-2HG production in cells[17,18]. Cells treated with nontargeting control small interfering RNA (siRNA) exhibited normoxic stabilization of HIF-1α when cultured in acidic medium supplemented with αKG (**Fig. 6f** and **Supplementary Fig. 11**). Ablation of either LDHA or MDH2 alone partially impaired stabilization of HIF-1α in response to acidification (**Supplementary Figs. 12a**,**b** and **13**). However, combined targeting of both LDHA and MDH2 abrogated L-2HG production (**Supplementary Fig. 12c**) and abolished the ability of cells to stabilize HIF-1α in response to acidification (**Fig. 6f** and **Supplementary Fig. 11**). These findings demonstrate that acid-enhanced conversion of αKG to L-2HG by LDHA and MDH2 is sufficient to stabilize HIF-1α in the absence of hypoxia.

DISCUSSION

Herein we demonstrate that LDH and MDH enzymes catalyze promiscuous enzymatic reduction of the alternative substrate αKG to L-2HG. Decades-old studies demonstrated alternative substrate use by dehydrogenase enzymes but lacked techniques to accurately assess the identity and chirality of metabolite products[26,27]. Our findings indicate that there are multiple enzymes that can reduce αKG to 2HG and that the chirality of 2HG is dictated by the specific enzyme involved. For example, LDH and MDH enzymes catalyze stereospecific production of L-2HG, whereas wild-type (and mutant) IDH and PHGDH catalyze stereospecific production of D-2HG.

The findings presented here substantiate prior genetic evidence implicating LDH and MDH as cellular sources of L-2HG[16–18,21]. In hypoxia, cells selectively produce L-2HG in a manner primarily

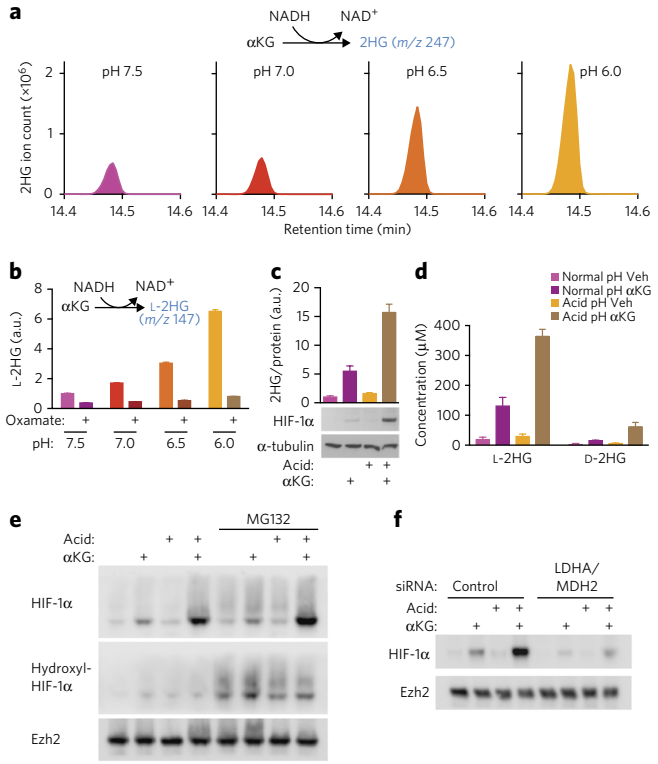

Figure 6 | Acid-enhanced production of L-2HG stabilizes HIF-1α. (**a**) SFXL cells were lysed in nondenaturing conditions at the indicated pH. Cell lysates were incubated for 16 h with 1 mM αKG and 0.22 mM NADH. Total 2HG was analyzed by GC–MS. (**b**) Lysate reactions were prepared as in **a** with addition of either vehicle (water) or 1 mM oxamate. L-2HG was measured by chiral LC–MS. Data are shown as the mean ± s.d. for triplicate reactions. (**c**) SFXL cells were cultured for 24 h in standard DMEM or DMEM titrated to pH 6.0 ('acid') with vehicle or 5 mM cell-permeable dimethyl-αKG. Total 2HG was measured by GC–MS. Data are shown as the mean ± s.d. for triplicate wells. (**d**) Quantification of intracellular L- and D-2HG concentrations by LC–MS (Online Methods). Data are shown as the mean ± s.d. of a total of six replicates per condition from two independent experiments. Veh, vehicle. (**e**) 293T cells were cultured for 24 h as in **c** with addition of vehicle or 10 μM MG132 for the final 1 h. Western blotting of nuclear extracts shows HIF-1α, hydroxyl-HIF-1α, and Ezh2 (loading control). (**f**) LDHA and MDH2 were targeted by siRNAs in SFXL cells followed by culture for 24 h as in **c**. The Western blots for **c** used whole-cell lysates, while those in **e** and **f** used nuclear extracts. Full blot images for **c**, **e**, and **f** are shown in **Supplementary Figure 11**. Results in **a**–**c** and **e** are representative of ≥3 independent experiments. Results in **f** are representative of two independent experiments.

dependent on LDHA and MDH2 (refs. 17,18). The relative contributions of LDHA and MDH2 to hypoxia-induced L-2HG appear to vary depending on the type of cell, which may be related to enzyme levels and subcellular pools of substrate. Hypoxic cells undergo a variety of metabolic changes that might favor L-2HG production[18,22–25,45]. Here we identify acidification and increased αKG concentration as factors that are sufficient to induce cellular production of L-2HG in normoxia. Indeed, *in vitro* enzymatic assays demonstrate that the promiscuous enzymatic activity of LDH, and to a lesser extent MDH, is enhanced by acidic pH, resulting in more efficient reduction of αKG to L-2HG. Acidic pH appears to enhance LDHA-mediated reduction of αKG by driving equilibrium toward the protonated state of the carboxylate tail, which permits docking of αKG via interaction with the Q100 residue in LDHA. Intracellular acidification might also explain, at least in part, the increased L-2HG observed in cells with electron-transport-chain dysfunction[46].

In hypoxia, L-2HG can function as a metabolic signaling molecule that mediates physiologic responses to help cells adapt to oxygen limitation[17,18]. L-2HG acts to stabilize HIF by inhibiting the αKG-dependent prolyl hydroxylases that target HIF for degradation[11,13]. Whether HIF-1α stabilization is a qualitatively or quantitatively unique property of L-2HG as compared to D-2HG remains controversial[13,47,48]. We have identified acidosis as a previously unappreciated physiologic stimulus that enhances conversion of αKG to L-2HG, resulting in robust stabilization of HIF-1α in normoxia. HIF-1α facilitates cellular adaptation to an acid load by inducing expression of carbonic anhydrases[49], and our findings suggest that acid-enhanced production of L-2HG may be part of this signaling axis. Indeed, we find that ablation of LDHA and MDH2 abrogates the ability of acidotic cells to stabilize HIF-1α. It is also possible that acidification and L-2HG cooperate in the stabilization of HIF-1α (ref. 50). In comparison to L-2HG, we observed approximately tenfold lower intracellular concentrations of D-2HG. Given that L-2HG functions as a more potent inhibitor of αKG-dependent enzymes than D-2HG[11–13], we conclude that D-2HG derived from wild-type IDH and/or PHGDH is negligible and likely does not play a physiologic role in this setting.

Promiscuous enzymatic activity results in the production of numerous metabolites that have been described as 'metabolite damage' or mistakes[10]. However, emerging evidence suggests that L-2HG, a metabolite produced by promiscuous enzyme activity, might represent a conserved metabolic response to multiple environmental stimuli including hypoxia and acidosis. L-2HG appears to mediate its effects through both HIF-dependent and HIF-independent mechanisms[17,18]. Future investigations will be directed at elucidating the mechanisms whereby L-2HG regulates physiologic responses to hypoxia and acidosis, as well as how deregulation of L-2HG metabolism might contribute to oncogenesis[14,15].

Received 16 June 2016; accepted 15 December 2016;
published online 6 March 2017

METHODS

Methods, including statements of data availability and any associated accession codes and references, are available in the online version of the paper.

References

1. Losman, J.A. & Kaelin, W.G. Jr. What a difference a hydroxyl makes: mutant IDH, (*R*)-2-hydroxyglutarate, and cancer. *Genes Dev.* **27**, 836–852 (2013).
2. Pavlova, N.N. & Thompson, C.B. The emerging hallmarks of cancer metabolism. *Cell Metab.* **23**, 27–47 (2016).
3. Dang, L. *et al.* Cancer-associated *IDH1* mutations produce 2-hydroxyglutarate. *Nature* **462**, 739–744 (2009).
4. Ward, P.S. *et al.* The common feature of leukemia-associated *IDH1* and *IDH2* mutations is a neomorphic enzyme activity converting α-ketoglutarate to 2-hydroxyglutarate. *Cancer Cell* **17**, 225–234 (2010).
5. Figueroa, M.E. *et al.* Leukemic *IDH1* and *IDH2* mutations result in a hypermethylation phenotype, disrupt TET2 function, and impair hematopoietic differentiation. *Cancer Cell* **18**, 553–567 (2010).
6. Lu, C. *et al. IDH* mutation impairs histone demethylation and results in a block to cell differentiation. *Nature* **483**, 474–478 (2012).
7. Sasaki, M. *et al.* IDH1(R132H) mutation increases murine haematopoietic progenitors and alters epigenetics. *Nature* **488**, 656–659 (2012).
8. Kats, L.M. *et al.* Proto-oncogenic role of mutant IDH2 in leukemia initiation and maintenance. *Cell Stem Cell* **14**, 329–341 (2014).
9. Saha, S.K. *et al.* Mutant IDH inhibits HNF-4α to block hepatocyte differentiation and promote biliary cancer. *Nature* **513**, 110–114 (2014).
10. Linster, C.L., Van Schaftingen, E. & Hanson, A.D. Metabolite damage and its repair or pre-emption. *Nat. Chem. Biol.* **9**, 72–80 (2013).
11. Chowdhury, R. *et al.* The oncometabolite 2-hydroxyglutarate inhibits histone lysine demethylases. *EMBO Rep.* **12**, 463–469 (2011).

12. Xu, W. *et al.* Oncometabolite 2-hydroxyglutarate is a competitive inhibitor of α-ketoglutarate-dependent dioxygenases. *Cancer Cell* **19**, 17–30 (2011).
13. Koivunen, P. *et al.* Transformation by the (*R*)-enantiomer of 2-hydroxyglutarate linked to EGLN activation. *Nature* **483**, 484–488 (2012).
14. Haliloglu, G. *et al.* L-2-hydroxyglutaric aciduria and brain tumors in children with mutations in the *L2HGDH* gene: neuroimaging findings. *Neuropediatrics* **39**, 119–122 (2008).
15. Shim, E.H. *et al.* L-2-Hydroxyglutarate: an epigenetic modifier and putative oncometabolite in renal cancer. *Cancer Discov.* **4**, 1290–1298 (2014).
16. Rzem, R. *et al.* A mouse model of L-2-hydroxyglutaric aciduria, a disorder of metabolite repair. *PLoS One* **10**, e0119540 (2015).
17. Intlekofer, A.M. *et al.* Hypoxia induces production of L-2-hydroxyglutarate. *Cell Metab.* **22**, 304–311 (2015).
18. Oldham, W.M., Clish, C.B., Yang, Y. & Loscalzo, J. Hypoxia-mediated increases in L-2-hydroxyglutarate coordinate the metabolic response to reductive stress. *Cell Metab.* **22**, 291–303 (2015).
19. Chen, C. *et al.* Cancer-associated IDH2 mutants drive an acute myeloid leukemia that is susceptible to Brd4 inhibition. *Genes Dev.* **27**, 1974–1985 (2013).
20. Simon, M.C. & Keith, B. The role of oxygen availability in embryonic development and stem cell function. *Nat. Rev. Mol. Cell Biol.* **9**, 285–296 (2008).
21. Rzem, R., Vincent, M.F., Van Schaftingen, E. & Veiga-da-Cunha, M. L-2-Hydroxyglutaric aciduria, a defect of metabolite repair. *J. Inherit. Metab. Dis.* **30**, 681–689 (2007).
22. Garofalo, O., Cox, D.W. & Bachelard, H.S. Brain levels of NADH and NAD^+ under hypoxic and hypoglycaemic conditions *in vitro*. *J. Neurochem.* **51**, 172–176 (1988).
23. Wise, D.R. *et al.* Hypoxia promotes isocitrate dehydrogenase–dependent carboxylation of α-ketoglutarate to citrate to support cell growth and viability. *Proc. Natl. Acad. Sci. USA* **108**, 19611–19616 (2011).
24. Bright, C.M. & Ellis, D. Intracellular pH changes induced by hypoxia and anoxia in isolated sheep heart Purkinje fibres. *Exp. Physiol.* **77**, 165–175 (1992).
25. Yan, G.X. & Kléber, A.G. Changes in extracellular and intracellular pH in ischemic rabbit papillary muscle. *Circ. Res.* **71**, 460–470 (1992).
26. Meister, A. Reduction of αγ-diketo and α-keto acids catalyzed by muscle preparations and by crystalline lactic dehydrogenase. *J. Biol. Chem.* **184**, 117–129 (1950).
27. Schatz, L. & Segal, H.L. Reduction of α-ketoglutarate by homogeneous lactic dehydrogenase X of testicular tissue. *J. Biol. Chem.* **244**, 4393–4397 (1969).
28. Struys, E.A., Jansen, E.E., Verhoeven, N.M. & Jakobs, C. Measurement of urinary D- and L-2-hydroxyglutarate enantiomers by stable-isotope-dilution liquid chromatography–tandem mass spectrometry after derivatization with diacetyl-L-tartaric anhydride. *Clin. Chem.* **50**, 1391–1395 (2004).
29. Pietrak, B. *et al.* A tale of two subunits: how the neomorphic R132H IDH1 mutation enhances production of αHG. *Biochemistry* **50**, 4804–4812 (2011).
30. Rendina, A.R. *et al.* Mutant IDH1 enhances the production of 2-hydroxyglutarate due to its kinetic mechanism. *Biochemistry* **52**, 4563–4577 (2013).
31. Leonardi, R., Subramanian, C., Jackowski, S. & Rock, C.O. Cancer-associated isocitrate dehydrogenase mutations inactivate NADPH-dependent reductive carboxylation. *J. Biol. Chem.* **287**, 14615–14620 (2012).
32. Fan, J. *et al.* Human phosphoglycerate dehydrogenase produces the oncometabolite D-2-hydroxyglutarate. *ACS Chem. Biol.* **10**, 510–516 (2015).
33. Mattaini, K.R. *et al.* An epitope tag alters phosphoglycerate dehydrogenase structure and impairs ability to support cell proliferation. *Cancer Metab.* **3**, 5 (2015).
34. Locasale, J.W. *et al.* Phosphoglycerate dehydrogenase diverts glycolytic flux and contributes to oncogenesis. *Nat. Genet.* **43**, 869–874 (2011).
35. Possemato, R. *et al.* Functional genomics reveal that the serine synthesis pathway is essential in breast cancer. *Nature* **476**, 346–350 (2011).
36. Terunuma, A. *et al.* MYC-driven accumulation of 2-hydroxyglutarate is associated with breast cancer prognosis. *J. Clin. Invest.* **124**, 398–412 (2014).
37. Zhu, A., Romero, R. & Petty, H.R. A sensitive fluorimetric assay for pyruvate. *Anal. Biochem.* **396**, 146–151 (2010).
38. Vesell, E.S. pH dependence of lactate dehydrogenase isozyme inhibition by substrate. *Nature* **210**, 421–422 (1966).
39. Wilks, H.M. *et al.* A specific, highly active malate dehydrogenase by redesign of a lactate dehydrogenase framework. *Science* **242**, 1541–1544 (1988).
40. Dunn, C.R. *et al.* Design and synthesis of new enzymes based on the lactate dehydrogenase framework. *Phil. Trans. R. Soc. Lond. B* **332**, 177–184 (1991).
41. Tokonami, N. *et al.* α-Ketoglutarate regulates acid–base balance through an intrarenal paracrine mechanism. *J. Clin. Invest.* **123**, 3166–3171 (2013).
42. Novoa, W.B., Winer, A.D., Glaid, A.J. & Schwert, G.W. Lactic dehydrogenase. V. Inhibition by oxamate and by oxalate. *J. Biol. Chem.* **234**, 1143–1148 (1959).
43. Schofield, C.J. & Ratcliffe, P.J. Oxygen sensing by HIF hydroxylases. *Nat. Rev. Mol. Cell Biol.* **5**, 343–354 (2004).
44. Finley, L.W. *et al.* SIRT3 opposes reprogramming of cancer cell metabolism through HIF1α destabilization. *Cancer Cell* **19**, 416–428 (2011).
45. Metallo, C.M. *et al.* Reductive glutamine metabolism by IDH1 mediates lipogenesis under hypoxia. *Nature* **481**, 380–384 (2011).
46. Mullen, A.R. *et al.* Oxidation of α-ketoglutarate is required for reductive carboxylation in cancer cells with mitochondrial defects. *Cell Rep.* **7**, 1679–1690 (2014).
47. Zhao, S. *et al.* Glioma-derived mutations in *IDH1* dominantly inhibit IDH1 catalytic activity and induce HIF-1α. *Science* **324**, 261–265 (2009).
48. Tarhonskaya, H. *et al.* Non-enzymatic chemistry enables 2-hydroxyglutarate-mediated activation of 2-oxoglutarate oxygenases. *Nat. Commun.* **5**, 3423 (2014).
49. Chiche, J. *et al.* Hypoxia-inducible carbonic anhydrase IX and XII promote tumor cell growth by counteracting acidosis through the regulation of the intracellular pH. *Cancer Res.* **69**, 358–368 (2009).
50. Mekhail, K., Gunaratnam, L., Bonicalzi, M.E. & Lee, S. HIF activation by pH-dependent nucleolar sequestration of VHL. *Nat. Cell Biol.* **6**, 642–647 (2004).

Acknowledgments

We thank members of the Thompson laboratory for helpful discussions. We thank M. Isik, S. Hanson, and A. Rizzi from the Chodera laboratory for assistance. A.M.I. was supported by the NIH/NCI (K08 CA201483-01A1), the Leukemia & Lymphoma Society (Special Fellow Award 3356-16), the Burroughs Wellcome Fund (Career Award for Medical Scientists 1015584), the Conquer Cancer Foundation of ASCO, the Susan and Peter Solomon Divisional Genomics Program, and the Steven A. Greenberg Fund. The work was also supported, in part, by the Leukemia & Lymphoma Society Specialized Center of Research Program (7011-16), the Starr Cancer Consortium (I6-A616), and grants from the NIH, including R01 CA168802-02 and R01 CA177828-02 (C.B.T.), K99 CA191021-01A1 (C.C.-F.), and the Memorial Sloan Kettering Cancer Center Support Grant (NIH P30 CA008748). M.R.G. and S.S. received financial support from the National Science Foundation (MCB 1022208) and infrastructure support from the National Institute on Minority Health and Health Disparities (8G12MD007603-29).

Author contributions

A.M.I. and C.B.T. conceived the project, designed the experiments, analyzed the data, and wrote the manuscript. A.M.I. and B.W. performed all of the experiments. H.L., H.S., and J.R.C. assisted with liquid chromatography–mass spectrometry. C.C.-F. assisted with intracellular pH measurement. A.S.R., S.S., M.R.G., and J.D.C. performed the computational modeling. All authors read and approved the manuscript.

Competing financial interests

The authors declare competing financial interests: details accompany the online version of the paper.

Additional information

Any supplementary information, chemical compound information and source data are available in the online version of the paper. Reprints and permissions information is available online at http://www.nature.com/reprints/index.html. Correspondence and requests for materials should be addressed to C.B.T.

ONLINE METHODS

Reagents. Purified enzymes were purchased from Sigma, including LDH from bovine heart (L2625), LDH from rabbit muscle (L2500), and MDH from porcine heart (M1567). Recombinant human enzymes were purchased from Abcam, including LDHA (ab93699), MDH1 (ab99244), MDH2 (ab99238), IDH1 (ab113858), and PHGDH (ab198455). Substrates, cofactors, and inhibitors were purchased from Sigma, including pyruvate, oxaloacetate, α-ketoglutarate, dimethyl-α-ketoglutarate, L-lactate, D-lactate, L-malate, D-malate, L-2-hydroxyglutarate, D-2-hydroxyglutarate, α-ketobutyrate, oxopentanoic acid, oxoadipic acid, ketohexanoic acid, phenylpyruvate, hydroxyphenylpyruvate, NADH, NADPH, and oxamate. FLAG-tagged wild-type and Q100R mutant LDHA constructs were cloned into the PCDNA3.1(+) vector (Addgene) by standard site-directed mutagenesis and verified by Sanger sequencing.

Cell culture. Adherent cell lines 293T (purchased from ATCC) and SFXL (SF188 cells with stable expression of Bcl-XL; generated as previously described[51]) were maintained at low passage number in high-glucose DMEM with 10% FBS, 25 mM glucose, 4 mM glutamine, 100 units/ml penicillin, and 100 μg/ml streptomycin and split every 2–3 d before reaching confluence. Cell lines were authenticated by short tandem repeat (STR) profiling. Cell lines repeatedly tested negative for mycoplasma throughout the experimental period. For siRNA experiments, cells were reverse-transfected with siRNA mixed with Lipofectamine RNAiMAX (Life Technologies) in Opti-MEM Reduced Serum Medium (Life Technologies) as described by the manufacturer. The following siRNAs (Thermo Fisher) were used: siLDHA = J-008201-06, target sequence: GGCAAAGACUAUAAUGUAA; siMDH2 = J-008439-12, target sequence: CGCCUGACCCUCUAUGAUA. For experiments with acidified medium, standard DMEM was titrated to pH 6.0 at room temperature and atmospheric oxygen and then filtered through a sterile 0.2-μm filter before use in tissue culture.

Western blotting. Cell lysates were extracted in 1× RIPA buffer (Cell Signaling), sonicated, and centrifuged at 21,000*g* at 4 °C, and supernatants were then collected. Nuclear extracts were prepared by harvesting cells in 50 mM NaCl, 0.5 M sucrose, 0.5% Triton X plus protease–phosphatase inhibitor cocktail (Thermo Fisher). Isolated nuclei were washed with 10 mM KCl and then lysed in 500 mM NaCl and 0.1% NP-40. Cleared cell lysates or nuclear extracts were quantified by BCA assay (Thermo Fisher) and normalized for total protein concentration. Samples were separated by SDS–PAGE, transferred to nitrocellulose membranes (Life Technologies), blocked in 5% milk prepared in Tris-buffered saline with 0.1% Tween 20 (TBST), incubated with primary antibodies overnight at 4 °C and then incubated with horseradish peroxidase (HRP)-conjugated secondary antibodies (GE Healthcare; anti-mouse, NA931V, sheep, 1:5,000; anti-rabbit, NA934V, donkey, 1:5,000) for 1 h the following day. After incubation with ECL (Thermo Fisher or GE Healthcare), imaging was performed using the Amersham Imager 600 (GE Healthcare). Primary antibodies used included anti-Ezh2 (Cell Signaling, 5246P; rabbit; 1:1,000), anti-HIF-1α (BD Biosciences, 610959; mouse; 1:200), anti-hydroxyl-HIF-1α (Cell Signaling, 3434P; rabbit; 1:1,000), anti-IDH1 (Proteintech, 12332-1-AP; rabbit; 1:1,000), anti-IDH2 (Abcam, ab55271; mouse; 1:1,000), anti-LDHA (Cell Signaling, 2012S; rabbit; 1:1,000), anti-MDH2 (Abcam, ab96193; rabbit; 1:1,000), anti-alpha-tubulin (Sigma, T9026: mouse; 1:5,000), and anti-vinculin (Abcam, ab18058; mouse; 1:1,000).

Intracellular pH measurement. Cells were loaded with either 5-(and-6)-carboxy, acetoxymethyl ester, acetate (SNARF-1; Thermo) or 2′,7′-*bis*-(2-carboxyethyl)-5-(and-6)-carboxyfluorescein, acetoxymethyl ester (BCECF; Thermo) ratiometric pH probes according to the manufacturer's instructions. After loading with pH probe, cells were incubated in DMEM without phenol red that was either left unmanipulated or titrated to pH 6.0 with addition of either DMSO (vehicle) or 5 mM dimethyl-αKG. After 4 h of incubation at 37 °C with 5% CO_2, fluorescence was measured using a plate reader (Tecan, Infinite M1000). The SNARF-1 probe was detected with a single excitation at 514 nm and a dual-emission ratio (580 nm and 640 nm). The BCECF probe was detected with a dual excitation (490 nm and 440 nm) and a fixed emission wavelength of 535 nm. Background fluorescence (cells without probes) was subtracted before all calculations. Intracellular pH was quantified by a standard curve ranging from pH 5.5 to pH 7.5 using DMEM with 10 μM nigericin and 10 μM valinomycin to equilibrate intracellular pH with extracellular pH.

Enzyme assays. Enzyme reactions were conducted in 33 mM potassium phosphate buffer titrated to pH 7.4, 7.0, 6.6, or 6.0. Purified enzymes were used at 5 units/ml, 1 μg/ml, or 10 μg/ml as indicated, and recombinant enzymes were used at 15 μg/ml unless otherwise indicated. FLAG-tagged wild-type and Q100R mutant LDHA enzymes were purified from transfected 293T cells using Anti-FLAG M2 Affinity Gel (Sigma) according to the manufacturer's instructions. FLAG-tagged enzymes were quantified by BCA assay and gel electrophoresis with Coomassie staining. NADH and NAPDH were used at 0.22 mM or 0.30 mM, respectively, throughout unless otherwise indicated. Substrates were used at 1 mM unless otherwise indicated. For NADH consumption assays, reactions were conducted in UV-transparent 96-well plates (Corning) with reaction volumes of 200 μl. A SpectraMax Plus 384 Microplate Reader (Molecular Devices) was used to monitor the absorbance at 340 nm every 30 s or 12 s throughout the course of the reaction. For each condition, the mean rate of NADH consumption for triplicate control reactions without enzyme was subtracted from the rate of NADH consumption for triplicate experimental reactions with enzyme. Reaction velocities were calculated using an extinction coefficient for NADH at ε340 of 6,220 $M^{-1}cm^{-1}$ and a path length of 0.56 cm for a 200-μl reaction volume in a standard 96-well plate. For NADH consumption assays with purified LDH and pyruvate, reactions were conducted in UV-transparent 3-ml cuvettes (BrandTech; path length 1 cm) with measurement of the absorbance at 340 nm every 2 s. For cell-lysate enzyme assays, SFXL cells were cultured in normoxic conditions in regular DMEM and harvested at subconfluence. The harvested cells were divided into four equal fractions, and nondenaturing cell lysates were prepared with PBS plus 0.1% Triton X titrated to pH 7.5, 7.0, 6.5, or 6.0 and used at either 50 or 100 μl per 200-μl reaction with αKG and NADH. The reaction mixtures were stopped after 16 h, at which time metabolites were extracted, derivatized, and analyzed by GC–MS or LC–MS.

Metabolite extraction and analysis. Metabolites were extracted with ice-cold 80:20 methanol:water containing 2 μM deuterated 2-hydroxyglutarate (D-2-hydroxyglutaric-2,3,3,4,4-d_5 acid; deuterated-2HG) as an internal standard. After overnight incubation at −80 °C, cell extract was harvested, sonicated, and centrifuged at 21,000*g* for 20 min at 4 °C to precipitate protein. Extracts were then dried in an evaporator (Genevac EZ-2 Elite). For GC–MS, metabolites were resuspended by addition of 50 μl of methoxyamine hydrochloride (40 mg/ml in pyridine) and incubated at 30 °C for 90 min with agitation. Metabolites were further derivatized by addition of 80 μl of MSTFA + 1% TCMS (Thermo Scientific) and 70 μl of ethyl acetate (Sigma) and incubated at 37 °C for 30 min. Samples were diluted 1:2 with 200 μl of ethyl acetate, then analyzed using an Agilent 7890A GC coupled to an Agilent 5975C mass selective detector. The GC was operated in splitless mode with constant helium carrier gas flow of 1 ml/min and with an HP-5MS column (Agilent Technologies). The injection volume was 1 μl, and the GC oven temperature was ramped from 60 °C to 290 °C over 25 min. Peaks representing compounds of interest were extracted and integrated using MassHunter software (Agilent Technologies) and then normalized to both the internal standard (deuterated-2HG) peak area and protein content as applicable. Ions used for quantification of metabolite levels were 2HG *m/z* 247 (confirmatory ion *m/z* 349), deuterated-2HG *m/z* 252 (confirmatory ion *m/z* 354), malate *m/z* 335 (confirmatory ions *m/z* 233, 245), and lactate *m/z* 190 (confirmatory ion *m/z* 219). Peaks were manually inspected and verified relative to known spectra for each metabolite.

For LC–MS, dried samples were derivatized with 100 μl of freshly prepared 50 mg/ml (+)-diacetyl-L-tartaric anhydride (DATAN, Sigma) in dichloromethane-acetic acid (v/v = 4:1) at 75 °C for 30 min. After cooling to room temperature, derivatized samples were dried under nitrogen at room temperature and resuspended in 200 μl of UltraPure water (18.2 MΩ, PureLab) before LC–MS/MS analysis. Analysis was performed on a Thermo Vantage triple-quadrupole mass spectrometer operating in SRM and negative ionization modes. LC separation was using an Acquity UPLC HSS T3 analytical column (2.1 × 100 mm, 1.8 μm, Waters) with an Agilent 1260 infinity binary pump. Mobile phase A

doi:10.1038/nchembio.2307

was 125 mg/l ammonium formate in water adjusted to pH 3.5 with formic acid, mobile phase B was methanol, and flow rate was 0.3 ml/min. Initial conditions were 3% B for 5 min, then increased to 80% B at 5.5 min and held for a further 2.5 min. 10 min of re-equilibration time was used to ensure retention time stability. The column temperature was held at 40 °C. Samples were kept at 4 °C and the injection volume was 5 µl. MS source parameters were as follows: spray voltage: 2,500 V; capillary temperature: 300 °C; vaporizer temperature: 250 °C; sheath gas pressure: 50 psi; aux gas pressure: 40 psi. Compound-specific S-lens values were as follows: 37 V (2HG), 36 V (malate), 34 V (lactate), 40 V (α-ketoglutarate), and 41 V (deuterated-2HG). Individual reactions were monitored and collision energies (CE) were as follows: 2HG *m/z* 363.0 → 147.1 (CE: 12 V)*, 129.1 (CE: 27 V); malate *m/z* 349.0 → 133.0 (CE: 14 V)*, 115.0 (CE: 28 V); lactate *m/z* 305.0 → 89.1 (CE: 14 V)*, α-ketoglutarate *m/z* 145.1 → 57.0 (CE: 12 V); 113.0 (CE: 16V); deuterated-2HG *m/z* 368.0 → 152.1 (CE: 13 V)*, 132.9 (CE: 22 V), with * indicating the primary transition used to quantify each metabolite. Pure standards of L-2HG, D-2HG, L-malate, D-malate, L-lactate, and D-lactate were derivatized and analyzed in parallel for each chiral determination experiment. The identities of metabolite enantiomers were determined by comparing to the retention times of the derivatized pure standards and additionally confirmed by spike-ins of derivatized pure standards into the experimental sample. Absolute metabolite quantification was performed using an external calibration curve with deuterated-2HG internal standard and the resulting concentrations corrected for the total cell volume extracted. Chromatograms were acquired and processed with XCalibur and TraceFinder software (Thermo Fisher).

Aqueous solution pK_a prediction. The aqueous solution pK_a values for the tail carboxylate moiety of αKG were predicted using Epik (Schrödinger release 2015-3)[52] using default settings.

Virtual docking of αKG to LDHA. Virtual docking of αKG was performed using Glide XP (Schrödinger release 2015-3)[53,54] to chain A of the 2.1-Å structure of lactate dehydrogenase A (LDHA; PDB identifier: 4OKN; ref. 55). Missing side chains were automatically constructed, amino acids were assigned protonation states compatible with a pH of 7.0 using the protein preparation wizard (Schrödinger release 2015-3), and crystallographic waters were removed. Bond orders for NADH were manually verified to avoid misassignment. Oxalate was used as a reference ligand to define the binding site, after adding fictitious atoms to ensure the minimum atom requirement for binding-site definition was met. Hydroxyl and thiol groups were allowed to rotate during grid generation. The tail-protonated form of αKG was docked in the presence of crystallographic NADH. Docking poses were minimized post-docking. The resulting conformations were clustered within a 0.5-Å r.m.s. deviation cutoff. This resulted in a single representative pose. All steps used default parameters unless otherwise noted. Poses and predicted hydrogen bonds were visualized using PyMOL.

Monte Carlo protonation state modeling using MCCE2 simulations. MCCE2 (ref. 56) was used to perform Monte Carlo simulations of amino acid side chain position and side chain and substrate protonation at equilibrium. The 2.3-Å structure of lactate dehydrogenase A (LDHA; PDB identifier 1I10; ref. 57) was used as input for all calculations (~60 computational hours on two Intel Xeon 2.40 GHz Six Core CPUs). αKG was modeled using a virtually docked pose from previous work[17]. This structure was prepared using the same docking procedure as detailed in this paper. The protonation states were compared between structures with the coenzyme and substrate (NADH and αKG) bound to LDHA or removed. The same starting protein structure was used for both bound and unbound types of simulation. The simulations were performed between pH 4.0–10.0 at intervals of 1.0 pH unit, and at pH 6.6 and 7.4. The total number of Monte Carlo steps for equilibration at each pH was 480,000. MCCE2 explores all side chain rotamers. DelPhi[58] was used to solve the Poisson–Boltzmann equation to obtain the pairwise interactions between charged and/or polar groups and the solvation energy with an internal dielectric constant of 4.0 and 80 for the solvent, with 0.15 salt concentration. The atomic partial charges and radii for the amino acids were obtained from PARSE[59], while AM1-BCC[60,61] charges for the ligands were generated by QUACPAC (OpenEye Toolkit 2016-Jun.1). MCCE2 calculates how the protein modifies the solution pK_a (p$K_{a,sol}$) of amino acids and substrates upon transfer into its position in the protein. NADH and αKG protonation states and tautomers, including their relative populations, were generated and performed using Epik (Schrödinger release 2015-3). Relative Epik energies were calculated at pH 4.0–10.0 at intervals of 1.0 pH unit, as well as pH 6.6 and 7.4. The energetic description for amino acids or standard ligands includes the p$K_{a,sol}$ as well as AMBER[62] torsion energies and van der Waals self-interactions. For the substrate, values were set to zero and the relative Epik energy of each tautomer and protonation state provided the starting reference state in solution. MCCE2 then calculated the shift in relative energy within the protein and thus showed the change in their distribution. The protein side chain rotamers and protonation states were sampled along with the ligand tautomers and protonation states at the given pH.

Data availability. The docking and MCCE2 calculation data, including scripts, have been deposited in "figshare" (https://dx.doi.org/10.6084/m9.figshare.4289894.v3). Inside the zip file, see the 'Docking' folder for files used in the docking procedures. Docking was performed using Maestro as part of Schrödinger release 2015-3. See the 'MCCE' folder for files used for the MCCE2 calculations for lactate dehydrogenase A. MCCE calculations were performed using MCCE2 (https://sites.google.com/site/mccewiki/install-mcce). Epik calculations were performed using Schrödinger release 2015-3. Referenced accession codes can be found in the Protein Data Bank under accession numbers 4OKN and 1I10.

51. Wise, D.R. *et al.* Myc regulates a transcriptional program that stimulates mitochondrial glutaminolysis and leads to glutamine addiction. *Proc. Natl. Acad. Sci. USA* **105**, 18782–18787 (2008).
52. Shelley, J.C. *et al.* Epik: a software program for pK_a prediction and protonation state generation for drug-like molecules. *J. Comput. Aided Mol. Des.* **21**, 681–691 (2007).
53. Friesner, R.A. *et al.* Glide: a new approach for rapid, accurate docking and scoring. 1. Method and assessment of docking accuracy. *J. Med. Chem.* **47**, 1739–1749 (2004).
54. Halgren, T.A. *et al.* Glide: a new approach for rapid, accurate docking and scoring. 2. Enrichment factors in database screening. *J. Med. Chem.* **47**, 1750–1759 (2004).
55. Kolappan, S. *et al.* Structures of lactate dehydrogenase A (LDHA) in apo, ternary and inhibitor-bound forms. *Acta Crystallogr. D Biol. Crystallogr.* **71**, 185–195 (2015).
56. Song, Y., Mao, J. & Gunner, M.R. MCCE2: improving protein pK_a calculations with extensive side chain rotamer sampling. *J. Comput. Chem.* **30**, 2231–2247 (2009).
57. Read, J.A., Winter, V.J., Eszes, C.M., Sessions, R.B. & Brady, R.L. Structural basis for altered activity of M- and H-isozyme forms of human lactate dehydrogenase. *Proteins* **43**, 175–185 (2001).
58. Yang, A.S., Gunner, M.R., Sampogna, R., Sharp, K. & Honig, B. On the calculation of pK_as in proteins. *Proteins* **15**, 252–265 (1993).
59. Cornell, W.D. *et al.* A second generation force field for the simulation of proteins, nucleic acids, and organic molecules. *J. Am. Chem. Soc.* **117**, 5179–5197 (1995).
60. Jakalian, A., Bush, B.L., Jack, D.B. & Bayly, C.I. Fast, efficient generation of high-quality atomic charges. AM1-BCC model: I. Method. *J. Comput. Chem.* **21**, 132–146 (2000).
61. Jakalian, A., Jack, D.B. & Bayly, C.I. Fast, efficient generation of high-quality atomic charges. AM1-BCC model: II. Parameterization and validation. *J. Comput. Chem.* **23**, 1623–1641 (2002).
62. Levitt, M. & Lifson, S. Refinement of protein conformations using a macromolecular energy minimization procedure. *J. Mol. Biol.* **46**, 269–279 (1969).